

PAPER

Predicting differential cross sections of electron scattering from tetrahydrofuran

To cite this article: Lulu Zhang *et al* 2017 *J. Phys. B: At. Mol. Opt. Phys.* **50** 085201

View the [article online](#) for updates and enhancements.

You may also like

- [Predicting differential cross sections of electron scattering from polyatomic molecules](#)
Weiguo Sun, Qi Wang, Yi Zhang *et al.*
- [Collisions of low- to intermediate-energy electrons with acetonitrile](#)
Victor A S da Mata, Milton M Fujimoto and Manoel G P Homem
- [Differential cross sections for projectile scattering angle in proton-helium collision at intermediate energies](#)
A Igarashi and D Kato



Easy-to-use and Helium-3 free
cryogenics solutions



LEARN MORE

Predicting differential cross sections of electron scattering from tetrahydrofuran

Lulu Zhang¹, Weiguo Sun^{1,2}, Yi Zhang³, Zhixiang Fan¹, Shide Hu¹ and Qunchao Fan²

¹Institute of Atomic and Molecular Physics, Sichuan University, Chengdu, Sichuan, 610065 People's Republic of China

²School of Science, Research Center for Advanced Computation, Xihua University, Chengdu, Sichuan, 610039 People's Republic of China

³College of OptoElectronic Science and Engineering, National University of Defense Technology, Changsha, Hunan, 410073 People's Republic of China

E-mail: swg@mail.xhu.edu.cn and wgsun@scu.edu.cn

Received 21 October 2016, revised 22 February 2017

Accepted for publication 2 March 2017

Published 29 March 2017



CrossMark

Abstract

A *difference algebraic converging method* for electron scattering from molecule (*DACMe*) is suggested based on the recently proposed difference converging method (DCM) to predict unknown differential cross sections (DCSs). The applications of the *DACMe* to electron scattering from tetrahydrofuran (THF) molecule at energies below 20 eV show that: (1) the *DACMe* DCSs excellently reproduce all the available experimental data; (2) the *DACMe* method correctly predicts unknown DCSs that may not be given experimentally; (3) the *DACMe* can be used as an economic and useful alternative method to predict the correct DCSs where such scattering data are required; (4) the *DACMe* method does not depend on the size and the stereochemistry structure of a scattering molecule; (5) the algebraic modification to the DCM enhances the computational efficiency of the DCM theoretical study by at least 110 times.

Supplementary material for this article is available [online](#)

Keywords: cross section, electron scattering, biomolecules, tetrahydrofuran

1. Introduction

Over the last decade, much attention has been paid to the investigation of low energy (<20 eV) electron interaction with the building blocks of DNA, since it could cause significant lesions to deoxyribonucleic acid (DNA), such as single and double strands break [1–4]. The interaction between electrons and biomolecules is also of great significance in the physical and biological fields, such as radiobiology [5–8]. Extensive research on electron scattering from components of DNA and ribonucleic acid (RNA) has been focused on measuring or calculating the differential cross sections (DCSs), the integral cross sections (ICSs) and the momentum transfer cross sections (MTCSs). The low energy electron scattering from an essential component of the DNA backbone and RNA [9, 10], the tetrahydrofuran (THF) molecule, a heterocyclic five-member hydrocarbon compound, has been widely studied, and much detailed data on

DCSs, ICSs and MTCSs has been obtained experimentally and theoretically [11–25].

Experimentally, the elastic DCSs for electron scattering from THF in the energy range of 6.5 to 50 eV have been measured using a crossed electron-target beam apparatus by Colyer *et al* [12], and the magnetic-angle-changing technique has been applied to measure the DCSs over the scattering angles of 20°–180° in the energy range of 6 to 20 eV [14]. Recently, Lemelin and coworkers reported the absolute cross sections for an energy range of 1 to 19 eV based on a high-resolution electron energy loss spectrometer [13]. It can be seen from these articles that the DCSs were measured at some angles, but were not given at other angles experimentally, and those missed DCSs may play indispensable roles in studying the interactions between electron and THF. Therefore, theorists have developed or applied some delicate quantum methods to calculate DCSs, ICSs and MTCSs for electron scattering from biomolecules in the last decade. For instance,

Winstead, McKoy and coworkers applied the Schwinger Multichannel (SMC) method and the Born corrected SMC method to calculate the DCSs, ICSs and MTCSs for an electron colliding with THF [18, 19]. The independent atom method (IAM) was applied to calculate DCSs and ICSs by Mozejko and Sanche [20]. Trevisan *et al* studied the DCSs and MTCSs using the complex Kohn variational method [21]. Fuss and coworkers obtained much theoretical cross section data using the IAM based on the screening-corrected additivity rule method [22]. Garland *et al* conducted a critical analysis of the experimental and theoretical cross sections, and proposed a full set of cross sections for scattering energies less than 300 eV of this scattering system [23].

The cross sections obtained from modern theoretical methods are usually calculated using scattering wave-functions and scattering potentials with given physical models. Delicate *ab initio* scattering studies are very useful in that they can usually help us understand the physics of many scattering systems, especially those systems where available scattering data from different research groups are in poor accord. On the other hand, although many quantum calculations have excellent agreement with experimental results for some scattering angles and energies using complicated and delicate scattering wave-functions and potentials, some fail to derive good results at other angles and energies using the same system wave-functions and scattering potentials as will be shown later. Particularly, when scattering angles (θ) are smaller than 20° (and in some cases when $\theta > 130^\circ$), experimental DCSs may not be available and the calculated DCSs of different theoretical methods may differ from each other. Therefore, such cases call for different scattering methods to address these problems.

Recently, Sun and coworkers proposed a *difference converging method* (DCM) to calculate the DCSs, ICSs and MTCSs for electron scattering from any molecules [26]. An analytical formula is developed in the DCM to establish a physical relation between the known experimental DCSs and an unknown one. The DCM theoretical calculations do not depend on the size and the stereochemistry structure of a scattering molecule and do not use any scattering wave-functions and scattering potentials, but rather use the DCM formula and a set of physical converging requirements. The DCM digs out almost all delicate quantum information and relevant physical effects which are internalized in the known experimental data rather than mimic this information through the use of basis parameters and physical models.

The DCM studies [26] on electron scattering from N_2 , H_2O , CH_4 and CF_3I molecules show that, although the DCM does not give a theoretical picture of scattering wave-functions and scattering potentials, it indeed reproduces all known experimental DCSs and correctly predicts unknown ones that may not be available experimentally or may not be correctly given theoretically.

The present work improves the computational efficiency of the DCM studies by introducing an algebraic technique to the DCM protocol, and applies the modified DCM to study the DCSs, ICSs and MTCSs of electron scattering from the

THF (C_4H_8O) target, which is a typical biomolecule and an important constituent of the DNA molecule.

In section 2, the DCM method will be outlined and the algebraic improvement on the DCM will be presented. Section 3 shows the applications and discussions. Section 4 gives the summary of this study.

2. Theoretical method

The quantum mechanical formula used to calculate the DCS functions $d(\theta)_{k_0}$ for electron-molecule scattering may be written as an expansion of the form [26–28],

$$d(\theta)_{k_0} \equiv 4k_0^2 \frac{d\sigma}{d\Omega}(k_0, \theta) = \sum_{L=0}^{L_{\max}} B_L P_L(\cos \theta) \quad (1)$$

where $(k_0^2/2) = E$ represents the energy of the incident electron, θ is the scattering angle, $P_L(\cos \theta)$ is the *Legendre* polynomial that is not a function of incident energy E [29], B_L is the angle-independent scattering coefficient that is essentially the function of incident energy and the interaction potentials between electron and molecule. In the following, the function $d(\theta)_{k_0}$ will be called a DCS for convenience. All scattering physics are included in these scattering coefficients. The lowest two coefficients B_0 and B_1 are directly related to the ICS $\sigma(k_0)$ and the MTCS $\sigma^m(k_0)$ by [28, 30],

$$\sigma(k_0) = \frac{\pi}{k_0^2} B_0 \quad (2)$$

$$\sigma^m(k_0) = \frac{\pi}{k_0^2} \left[B_0 - \frac{1}{3} B_1 \right] \quad (3)$$

where the scattering coefficients (B_0, B_1) can be evaluated using equations (A7) and (A11) of the supplemental data (SD) of [26].

Based on the fact that all experimental DCSs satisfy the physical equation (1), a DCM equation that bridges the measured DCSs and the unknown one is derived using multiple differences of DCSs in [26] as,

$$\begin{aligned} d(\theta_{16}) = & [d(\theta_1) - 2d(\theta_2)]T_1 + d(\theta_3)T_{2p} \\ & - d(\theta_4)T_{2q} + d(\theta_5)T_3 - d(\theta_6)T_4 \\ & + d(\theta_7)T_5 - d(\theta_8)T_6 + d(\theta_9)T_7 \\ & - d(\theta_{10})T_8 + d(\theta_{11})T_9 - d(\theta_{12})T_{10} \\ & + d(\theta_{13})T_{11} - d(\theta_{14})T_{12} + d(\theta_{15})T_{13}. \end{aligned} \quad (4)$$

The calculable expansion coefficients T_k and their related coefficients are defined in the SD of [26], and they are the functions of *Legendre* polynomials $P_L(\cos \theta)$. There are no mathematical approximations and physical models used in the derivation, and there are no experiential or unknown parameters in equation (4). One can predict an unknown DCS $d(\theta_{n+1})$ by using a set of physical converging requirements and n known experimental DCSs $[d(\theta_1), d(\theta_2), \dots, d(\theta_n)]$ for $n = 15$. The DCM equations similar to equation (4) are also given in the SD of [26] for $n < 15$.

Although previous DCM studies [26] on electron scattering from N_2 , H_2O , CH_4 and CF_3I molecules have obtained excellent theoretical DCSs, the computational process on a

normal PC is relatively time consuming due to the many algorithmic steps involved. This present study will modify the DCM method by introducing an algebraic performance in the DCM computational process, and will apply the modified method to study electron scattering from a biomolecule of THF (C_4H_8O) for the first time. The modification is described as follows:

The first mathematical difference $\Delta d_{i,k}$ between two physical DCSs $d(\theta_i)$ and $d(\theta_k)$ can be given from equation (1) as,

$$\begin{aligned} \Delta d_{i,k} = d(\theta_i) - d(\theta_k) = & B_0 P_0^{\theta_i} + B_1 P_1^{\theta_i} + B_2 P_2^{\theta_i} \\ & + \dots + B_{L_{\max}} P_{L_{\max}}^{\theta_i} - (B_0 P_0^{\theta_k} + B_1 P_1^{\theta_k} \\ & + B_2 P_2^{\theta_k} + \dots + B_{L_{\max}} P_{L_{\max}}^{\theta_k}) \end{aligned} \quad (5)$$

where $P_L^\theta \equiv P_L(\cos \theta_i)$ and $P_0^\theta = 1$. The coefficient B_0 can be expressed from equation (1) for $d(\theta_j)$ as,

$$B_0 = d(\theta_j) - B_1 P_1^{\theta_j} - B_2 P_2^{\theta_j} - \dots - B_{L_{\max}} P_{L_{\max}}^{\theta_j}. \quad (6)$$

Similarly, the second difference between the DCS differences $\Delta d_{1,2}$ and $\Delta d_{2,3}$ is,

$$\begin{aligned} d(\theta_1) - 2d(\theta_2) + d(\theta_3) = & B_1 P_1^{\theta_1} \\ & + B_2 P_2^{\theta_1} + \dots + B_{L_{\max}} P_{L_{\max}}^{\theta_1} \\ & - 2(B_1 P_1^{\theta_2} + B_2 P_2^{\theta_2} \\ & + \dots + B_{L_{\max}} P_{L_{\max}}^{\theta_2}) + (B_1 P_1^{\theta_3} \\ & + B_2 P_2^{\theta_3} + \dots + B_{L_{\max}} P_{L_{\max}}^{\theta_3}). \end{aligned} \quad (7)$$

Rearranging it, one can get B_1 for scattering angles $(\theta_1, \theta_2, \theta_3)$,

$$\begin{aligned} B_1 = & P_{11}^\theta [d(\theta_1) - 2d(\theta_2) + d(\theta_3)] - B_2 P_{12}^\theta \\ & - B_3 P_{13}^\theta - \dots - B_{L_{\max}} P_{1L_{\max}}^\theta \end{aligned} \quad (8)$$

where the functions P_{1k}^θ are

$$\begin{aligned} P_{11}^\theta &= \frac{1}{P_1^{\theta_1} - 2P_1^{\theta_2} + P_1^{\theta_3}}, \\ P_{12}^\theta &= \frac{P_2^{\theta_1} - 2P_2^{\theta_2} + P_2^{\theta_3}}{P_1^{\theta_1} - 2P_1^{\theta_2} + P_1^{\theta_3}}, \\ P_{13}^\theta &= \frac{P_3^{\theta_1} - 2P_3^{\theta_2} + P_3^{\theta_3}}{P_1^{\theta_1} - 2P_1^{\theta_2} + P_1^{\theta_3}}, \dots, \\ P_{1L_{\max}}^\theta &= \frac{P_{L_{\max}}^{\theta_1} - 2P_{L_{\max}}^{\theta_2} + P_{L_{\max}}^{\theta_3}}{P_1^{\theta_1} - 2P_1^{\theta_2} + P_1^{\theta_3}}. \end{aligned} \quad (9)$$

Now substituting the B_0 in equation (6) into the equation for $d(\theta_l)$,

$$\begin{aligned} d(\theta_l) = & (d(\theta_j) - B_1 P_1^{\theta_j} - B_2 P_2^{\theta_j} - \dots - B_{L_{\max}} P_{L_{\max}}^{\theta_j}) \\ & \times P_0^{\theta_l} + B_1 P_1^{\theta_l} + B_2 P_2^{\theta_l} + \dots + B_{L_{\max}} P_{L_{\max}}^{\theta_l} \\ d(\theta_l) = & d(\theta_j) + B_1 (P_1^{\theta_l} - P_1^{\theta_j}) + B_2 (P_2^{\theta_l} - P_2^{\theta_j}) \\ & + B_3 (P_3^{\theta_l} - P_3^{\theta_j}) + \dots + B_{L_{\max}} (P_{L_{\max}}^{\theta_l} - P_{L_{\max}}^{\theta_j}). \end{aligned} \quad (10)$$

Substituting the coefficient B_1 in equation (8) into the above equation,

$$\begin{aligned} d(\theta_l) = & d(\theta_j) + B_2 (P_2^{\theta_l} - P_2^{\theta_j}) + B_3 (P_3^{\theta_l} - P_3^{\theta_j}) \\ & + \dots + B_{L_{\max}} (P_{L_{\max}}^{\theta_l} - P_{L_{\max}}^{\theta_j}) + \{ [d(\theta_1) \\ & - 2d(\theta_2) + d(\theta_3)] P_{11}^\theta - B_2 P_{12}^\theta \\ & - B_3 P_{13}^\theta - \dots - B_{L_{\max}} P_{1L_{\max}}^\theta \} \\ & \times (P_1^{\theta_l} - P_1^{\theta_j}). \end{aligned}$$

Rearranging it, one has,

$$\begin{aligned} & B_2 (P_2^{\theta_l} - P_2^{\theta_j} - P_{12}^\theta P_1^{\theta_l} + P_{12}^\theta P_1^{\theta_j}) + B_3 (P_3^{\theta_l} - P_3^{\theta_j} \\ & - P_{13}^\theta P_1^{\theta_l} + P_{13}^\theta P_1^{\theta_j}) + \dots + B_{L_{\max}} (P_{L_{\max}}^{\theta_l} - P_{L_{\max}}^{\theta_j} \\ & - P_{1L_{\max}}^\theta P_1^{\theta_l} + P_{1L_{\max}}^\theta P_1^{\theta_j}) = d(\theta_l) - d(\theta_j) \\ & - [d(\theta_1) - 2d(\theta_2) + d(\theta_3)] P_{11}^\theta \\ & \times (P_1^{\theta_l} - P_1^{\theta_j}) \\ B_2 p(\theta_l)_2 + B_3 p(\theta_l)_3 + \dots + B_{L_{\max}} p(\theta_l)_{L_{\max}} = & d(\theta_l) \\ & - d(\theta_j) - [d(\theta_1) - 2d(\theta_2) + d(\theta_3)] P_{11}^\theta \\ & \times (P_1^{\theta_l} - P_1^{\theta_j}), \quad l \neq j. \end{aligned} \quad (11)$$

where

$$\begin{aligned} p(\theta_l)_i = & P_i^{\theta_l} - P_i^{\theta_j} - P_{1i}^\theta P_1^{\theta_l} + P_{1i}^\theta P_1^{\theta_j}, \\ & \{i = 2, 3, \dots, L_{\max}; l \neq j\}. \end{aligned} \quad (12)$$

The indices (l, j) are chosen such that $p(\theta_l)_i$ will not be zero. Equation (11) corresponds to a set of linear algebraic equations of $(L_{\max} - 1)$ unknown coefficients $(B_2, B_3, \dots, B_{L_{\max}})$ for given (l, j) , and can be rewritten as,

$$PB = D \quad (13)$$

where the $(L_{\max} - 1) \times (L_{\max} - 1)$ coefficient matrix P is

$$P = \begin{pmatrix} p(\theta_1)_2 & p(\theta_1)_3 & \dots & p(\theta_1)_{L_{\max}} \\ p(\theta_2)_2 & p(\theta_2)_3 & \dots & p(\theta_2)_{L_{\max}} \\ \vdots & \vdots & \vdots & \vdots \\ p(\theta_{L_{\max}-1})_2 & p(\theta_{L_{\max}-1})_3 & \dots & p(\theta_{L_{\max}-1})_{L_{\max}} \end{pmatrix}. \quad (14)$$

In equation (13), the column matrices B and D are

$$\begin{aligned} B = & \begin{pmatrix} B_2 \\ B_3 \\ \vdots \\ B_{L_{\max}} \end{pmatrix}, \\ D = & \begin{pmatrix} d(\theta_1) - d(\theta_j) - d(\theta_{123}) P_{11}^\theta (P_1^{\theta_1} - P_1^{\theta_j}) \\ d(\theta_2) - d(\theta_j) - d(\theta_{123}) P_{11}^\theta (P_1^{\theta_2} - P_1^{\theta_j}) \\ \vdots \\ d(\theta_{L_{\max}-1}) - d(\theta_j) - d(\theta_{123}) P_{11}^\theta (P_1^{\theta_{L_{\max}-1}} - P_1^{\theta_j}) \end{pmatrix} \end{aligned} \quad (15)$$

where $\theta_l \neq \theta_j$ and $d(\theta_{123}) = d(\theta_1) - 2d(\theta_2) + d(\theta_3)$. In the coefficient matrix P , all matrix elements $p(\theta_l)_i$ are the functions of Legendre polynomials $P_L^\theta \equiv P_L(\cos \theta_i)$. The elements of matrix D are the functions of experimental DCSs $d(\theta_i)$.

Therefore, one can easily solve algebraic equation (13) using a set of chosen experimental DCSs $[d(\theta_1), d(\theta_2), \dots, d(\theta_{L_{\max}-1}); d(\theta_j)]$ for unknown scattering coefficients $(B_2, B_3, \dots, B_{L_{\max}})$. The coefficients B_0 and B_1 can then be obtained using equations (6) and (8), respectively.

Since no orbital parameters of bases functions and potential models are used in the above derivations, the only errors introduced to the scattering information $(B_0, B_1, B_2, \dots, B_{L_{\max}})$ are those from known experimental DCSs. One may use $\partial d(\theta_j)$ denoting the error of the experimental DCS $d(\theta_j)$ and ∂B_i for that of B_i . The error in equation (11) may be written as

$$\begin{aligned} & \partial B_2 p(\theta_1)_2 + \partial B_3 p(\theta_1)_3 + \dots + \partial B_{L_{\max}} p(\theta_1)_{L_{\max}} \\ &= \partial d(\theta_1) - \partial d(\theta_j) - [\partial d(\theta_1) - 2\partial d(\theta_2) \\ &+ \partial d(\theta_3)] P_{11}^\theta (P_1^\theta - P_1^{\theta_j}) = \partial d(\theta_1) \\ &- \partial d(\theta_j) - \partial \tilde{d} p(\theta_1)_i \end{aligned} \quad (16)$$

where

$$\begin{aligned} & \partial \tilde{d} = \partial d(\theta_1) - 2\partial d(\theta_2) + \partial d(\theta_3), \\ & p(\theta_1)_i = P_{11}^\theta (P_1^{\theta_i} - P_1^{\theta_j}). \end{aligned} \quad (17)$$

To have minimum errors on the right hand side (RHS) of equation (16), one may require that the known coefficients $\{p(\theta_1)_2, p(\theta_1)_3, \dots, p(\theta_1)_{L_{\max}}\}$ on the left hand side are minimum because one may not know the values of errors $(\partial B_2, \partial B_3, \dots, \partial B_{L_{\max}})$.

Since solving the DCM equation (4) involves many more interim algorithmic steps than solving the algebraic equation (13), one may choose the latter to greatly enhance the computational efficiency. Because one will use $d(\theta_j)$ and $(L_{\max} - 1)$ other experimental-based data $d(\theta_l)$ ($l = 1, 2, \dots, L_{\max} - 1; l \neq j$) in the matrix D of equation (15), one should choose L_{\max} $d(\theta_i)$ from m known experimental data when solving equation (13). Therefore one will solve equation (13) $N = C_m^{L_{\max}}$ times. Since there are $C_m^{L_{\max}}$ [$L_{\max} < m$] ways to choose L_{\max} experimental DCSs out of the m known ones, therefore, one may obtain L_{\max} mathematical solutions of scattering information $(B_0, B_1, B_2, \dots, B_{L_{\max}})$ by solving equation (13). One can find the best physical solution from the $C_m^{L_{\max}}$ ones using the following converging requirements:

$$\begin{aligned} & \text{Max} \{p(\theta_1)_2, p(\theta_1)_3, \dots, p(\theta_1)_{L_{\max}}\} \\ & \rightarrow \text{sufficiently small} \end{aligned} \quad (18)$$

$$\max |d(\theta_l)_{\text{cal}} - d(\theta_l)_{\text{exp}l}| \rightarrow 0 \quad (19)$$

$$\max \left| \frac{d(\theta_l)_{\text{cal}} - d(\theta_l)_{\text{exp}l}}{d(\theta_l)_{\text{exp}l}} \right| \rightarrow 0 \quad (20)$$

$$|\sigma(k)_{\text{exp}l} - \sigma(k)_{\text{cal}}| \rightarrow 0 \quad (21)$$

$$|\sigma^m(k)_{\text{exp}l} - \sigma^m(k)_{\text{cal}}| \rightarrow 0 \quad (22)$$

where equation (18) says that the maximum value of the $(L_{\max} - 1)$ coefficients $p(\theta_1)_i$ should be as small as possible such that the errors of the known experimental DCSs on the RHS of equation (16) are minimum. Equations (19) and (20) require that the calculated

DCSs $d(\theta_l)_{\text{cal}}$ converge with each corresponding experimental counterpart $d(\theta_l)_{\text{exp}l}$. Equations (21) and (22) require that the theoretical ICSs and MTCSs obtained using equations (2) and (3) should converge with the experimental ones.

When the best converged scattering coefficients $(B_0, B_1, B_2, \dots, B_{L_{\max}})$ are obtained, one has the best physical representation of the experimental DCSs and therefore can use such information to predict the unknown DCSs. The accuracy of the predicted DCSs $d(\theta_l)_{\text{cal}}$ uniquely depends on the integrity and the accuracies of the known experimental DCSs. Since a multiple mathematical *difference* method, an *algebraic* method and a set of physical *converging* standards are used in above protocol to obtain correct scattering information and thereafter to predict unknown DCSs, one may call such a method the *difference algebraic converging method* for electron scattering from molecule (*DACMe*), and call the obtained theoretical DCSs the *DACMe* DCSs $d(\theta_l)_{\text{cal}} (\equiv d(\theta_l)_{\text{DACMe}})$.

The *DACMe* is not explicitly molecular structure dependent, and not explicitly electronic state and scattering potential dependent. All molecular structure, electronic state and delicate scattering information is included in the experimental DCSs and in the scattering coefficients B_k 's. Therefore, the *DACMe* can be applied to study the DCSs of electron scattering from any molecule where experimental data are not available.

3. Applications and discussions

The *DACMe* method is applied to study the DCSs, ICSs and MTCSs of low energy electron scattering from a THF molecule based on an experimental study [14] for scattering energies of 6, 7, 8, 10, 12, 15 and 20 eV, and based on recent measurements [12] for 8 and 20 eV respectively. Dampc and coworkers [14] presented experimental DCSs for scattering angles $\theta_{\text{cal}} \rightarrow 180^\circ$, and Colyer *et al* [12] reported their measured DCSs in the $\theta_{\text{cal}} < \theta^\circ < 130^\circ$ angular region. The experimental ICSs $\sigma(k)_{\text{exp}l}$ and the MTCSs $\sigma^m(k)_{\text{exp}l}$ used to converge the *DACMe* calculations as given in equations (21) and (22) were generated by integrating the normalized SMC DCSs (which are not given in the experiment) of $0^\circ \rightarrow \theta_{\text{cal}}^\circ$ [18, 19] and the experimental DCSs of $\theta_{\text{cal}}^\circ \rightarrow 180^\circ$ [14]. Winstead and McKoy [18] presented their calculated SMC DCSs without Born corrections for dipole potentials while Gauf and coworkers [19] included the Born corrections in their SMC DCSs. The converged *DACMe* scattering coefficients B_k are listed in table A1, available at stacks.iop.org/JPB/50/085201/mmedia of the SD of the present study for scattering energies of 6, 7, 8, 10, 12, 15 and 20 eV [14]. The experimental DCSs and the *DACMe* results are tabulated in tables A2–A8 of the SD, and are plotted in figures 1–7 with relevant quantum scattering calculations, respectively. In these figures, the dot-dashed curve (—·—) gives the SMC DCSs [18] without Born correction for dipole scattering potential. The dashed curve (— —) shows the Born corrected SMC DCSs [19]. The solid curve (—) is the *DACMe* DCSs

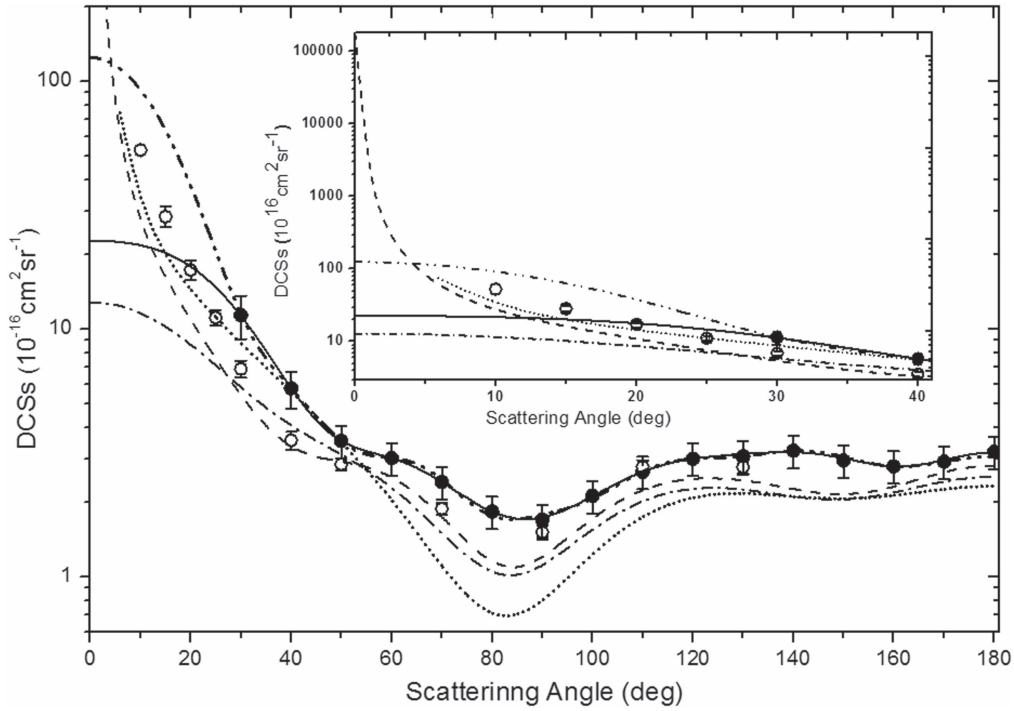


Figure 1. Elastic DCSs of $e + \text{THF}$ at 6 eV. Full circles (●), experiment data of Dampc *et al* [14]; hollow circles (○), experiment data of Gauf *et al* [19]; black solid curve (—), presents *DACMe* obtained using SMC amended experimental ICS1 and MTCS1 as converging requirements; double-dots-dashed curve (— · —), presents Born corrected *DACMe* obtained using Born SMC amended experimental ICS2 and MTCS2 as converging requirements; dot-dashed curve (— · · —), SMC calculation [18]; dashed curve (— —), Born corrected SMC calculations [19]; dotted curve (···), from the complex Kohn variational method [21].

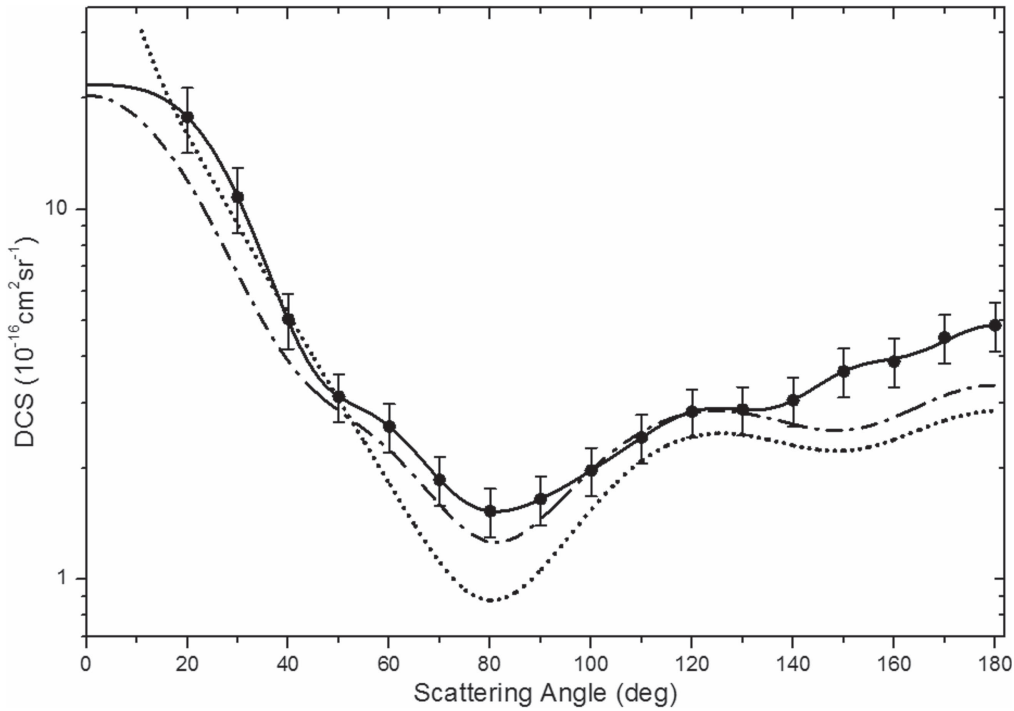


Figure 2. Elastic DCSs of $e + \text{THF}$ at 7 eV. Full circles (●), experiment data of Dampc *et al* [14]; solid curve (—), presents *DACMe* (without Born correction) obtained using SMC amended experimental ICS1 and MTCS1 as converging requirements; dot-dashed curve (— · · —), SMC calculation [18]; dotted curve (···), from the complex Kohn variational method [21].

obtained using the SMC amended experimental (full) ICS1 and MTCS1 without Born correction as converging requirements. The double-dots-dashed curve (— · —) presents the

Born corrected *DACMe* obtained using Born SMC amended experimental (full) ICS2 and MTCS2 as converging requirements. The dotted curve (···) gives the DCSs of the complex

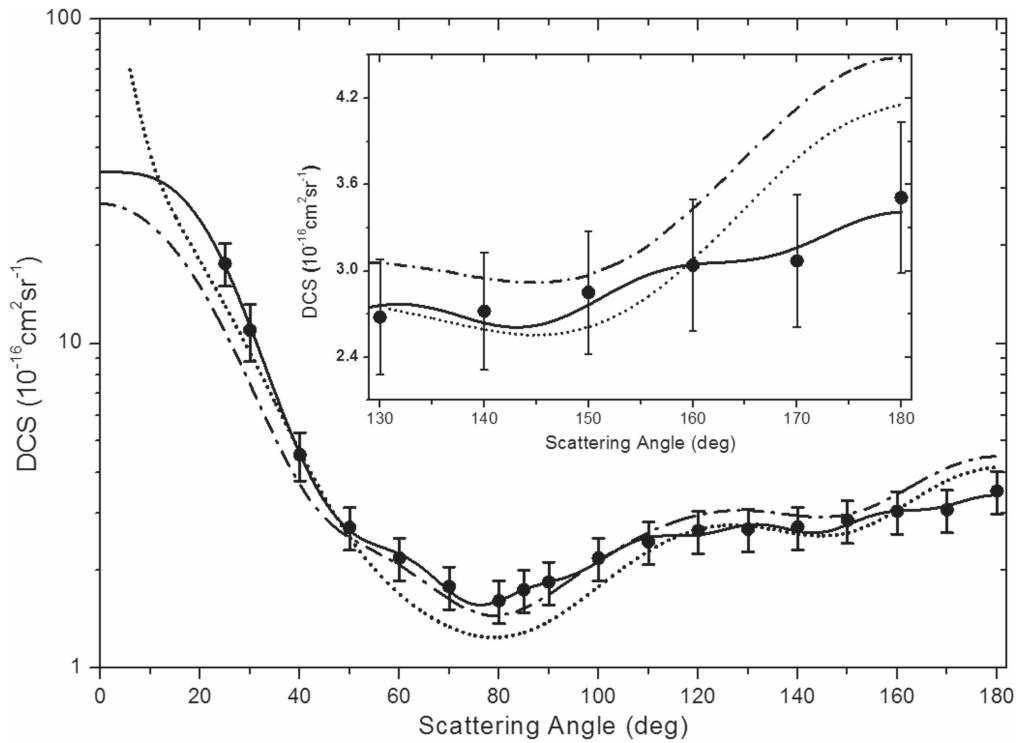


Figure 3. Elastic DCSs of $e + \text{THF}$ at 8 eV. All notations are as those in figure 2.

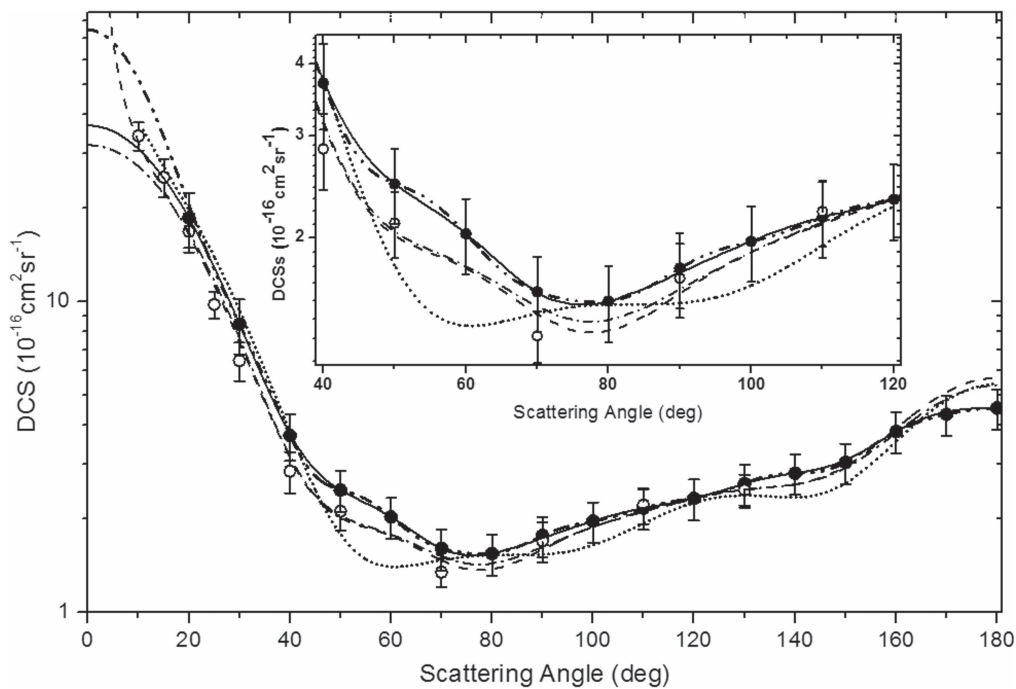


Figure 4. Elastic DCSs of $e + \text{THF}$ at 10 eV. All notations are as those in figure 1.

Kohn variational method [21]. The comparative studies indicate that the computational speed of the *DACMe* converging studies is at least 110 times faster than that of the original DCM for every scattering energy.

Table A2 and figure 1 show that both the *DACMe* DCSs without Born correction (—) and those with Born correction (double-dots-dashed curve (— · — · —)) excellently reproduce all recently measured data (●) at 6 eV [14], and correctly present

the detailed physical shape of the experimental DCSs. The Born corrected *DACMe* DCSs (double-dots-dashed curve (— · — · —)) correctly predict the values and physical shape of all DCSs for $\theta^\circ < 30^\circ$ which are not given by the experimental study [14]. The agreement between the experimental DCSs and both *DACMe* data is much better than that between the experiment and the SMC DCSs or the Born corrected SMC DCSs (‘— · — · —’ [18] or ‘— — —’ [19]), and that between the

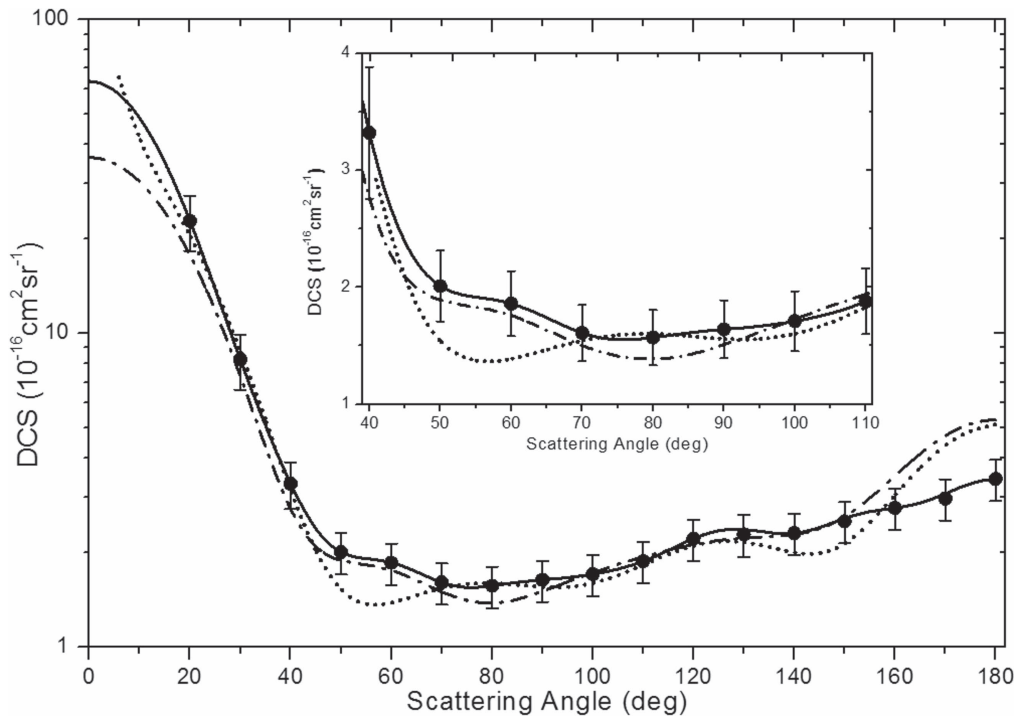


Figure 5. Elastic DCSs of $e + \text{THF}$ at 12 eV. All notations are as those in figure 2.

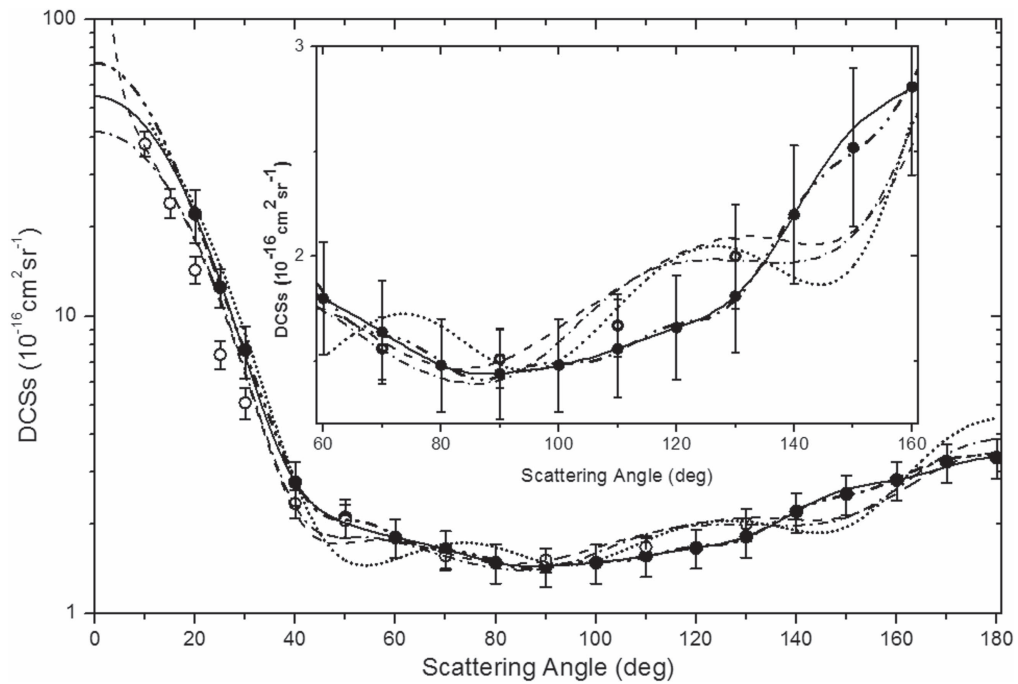


Figure 6. Elastic DCSs of $e + \text{THF}$ at 15 eV. All notations are as those in figure 1.

experiment and the complex Kohn DCSs (...) [21]. The inset indicates that the Born corrected SMC DCSs (—) heavily overestimate the DCSs of $\theta^\circ < 10^\circ$, particularly for scattering angles $\theta^\circ < 3^\circ$. The correctness of the predicted *DACMe* DCSs can also be seen from the small relative percent error (0.06%) of present (Born corrected) *DACMe* ICS (72.41) from the Born *DACMe* amended experimental ICS (72.45) in table 1. This picture can also be seen from the MTCS data in table 2.

Figures 2–7 and tables A3–A8 present similar physical pictures for 7, 8, 10, 12, 15 and 20 eV as that of 6 eV, respectively. These figures and tables indicate that the *DACMe* DCSs (—) have better agreement with the experimental ones (●) [14] than the SMC and the Born corrected SMC (‘— —’ [18] and ‘— —’ [19]) and the complex Kohn DCSs (...) [21].

The experiment curves and all theoretical DCS curves are in similar shape in figure 2 at 7 eV and in figure 3 at 8 eV to

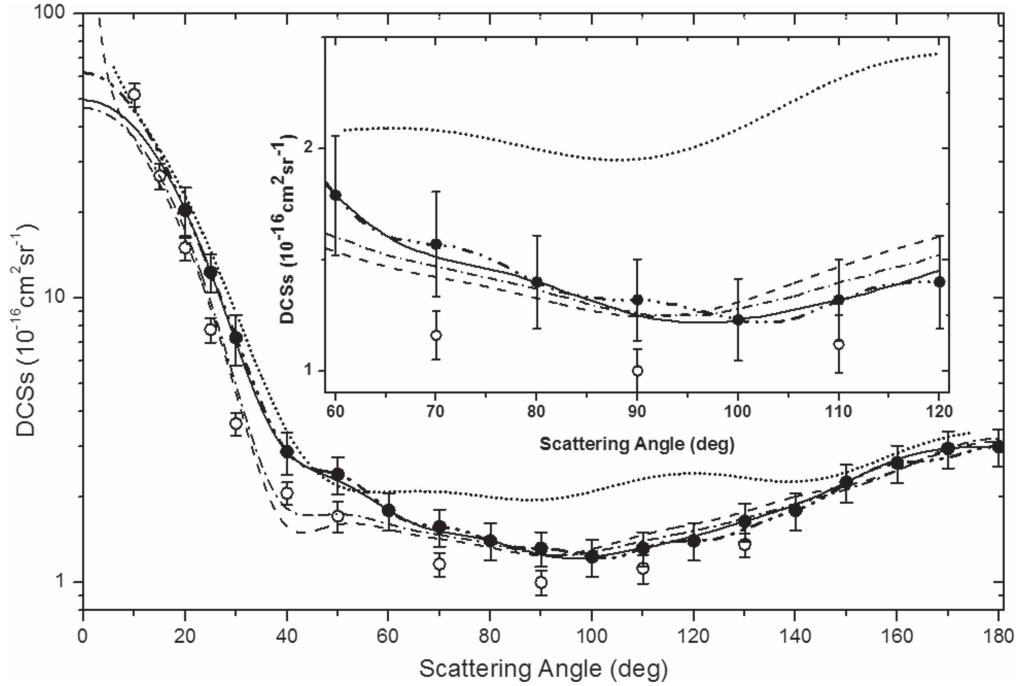


Figure 7. Elastic DCSs of $e + \text{THF}$ at 20 eV. All notations are as those in figure 1.

the case in figure 1. There are no Born corrected SMC calculations available for these two energies. In figure 2 the DCSs of the SMC and the complex Kohn are quite smaller than both the experimental and the *DACMe* ones at backward scattering of $\theta^\circ > 145^\circ$, and in figure 3 the former two are evidently greater than the latter for $\theta^\circ > 160^\circ$.

All theoretical studies give good results in figure 4 at 10 eV and in figure 5 at 12 eV (and in table A5 and in table A6), but the Born corrected SMC at 10 eV shows a too strong forward scattering peak for $\theta^\circ < 10^\circ$ (up to $106\,000 \times 10^{-16} \text{ cm}^2 \text{ sr}^{-1}$ at about $\theta^\circ = 0^\circ$) compared to that in figure 1. There are also no Born corrected SMC data for 12 eV. The SMC and the complex Kohn show a higher backward scattering tail for $\theta^\circ > 160^\circ$ in figure 5. The SMC with Born-dipole correction and the complex Kohn DCSs in figure 6 present an evident f -wave scattering feature at 15 eV, however the experiment and both the *DACMe* (—) and the Born corrected *DACMe* (in table A7 and in double-dots-dashed curve) data show a clear p -wave scattering feature. Finally, table A8 and figure 7 indicate that both the experiment and the *DACMe* DCSs have p -wave dominated scattering at 20 eV, instead of d -wave and f -wave mixed scattering as given by the SMC and the complex Kohn results.

Table 1 presents experimental-based ICSs, theoretical *DACMe* ICSs and relative percent error of each scattering energy, respectively. Table 2 gives similar comparative data for MTCSs. The SMC amended experimental (full) ICSs and MTCSs consisted of integrating the normalized SMC DCSs of $0^\circ \rightarrow \theta_{\text{cal}}^\circ$ [18, 19] and the experimental DCSs of $\theta_{\text{cal}}^\circ \rightarrow 180^\circ$ [14]. The angle $\theta_{\text{cal}}^\circ$ is indicated in both tables for every energy. The cross sections obtained from integrating the experimental DCSs of $\theta_{\text{cal}}^\circ \rightarrow 180^\circ$ will be called the experimental partial ICSs or MTCSs [14], and are given in bold in

the second column of both tables 1 and 2, and the ones in the third column are the SMC amended experimental (full) ICS1 or MTCS1. The fourth column presents the Born SMC amended experimental (full) ICS2 or MTCS2.

For comparison, the Born *DACMe* amended experimental (full) ICS3 and MTCS3 are evaluated by integrating the Born corrected *DACMe* DCSs of 0° to $\theta_{\text{cal}}^\circ$ and the experimental DCSs of $\theta_{\text{cal}}^\circ$ to 180° [14], and listed in bold in the fifth column of both tables. The contributions of the Born *DACMe* DCSs of $0^\circ \rightarrow \theta_{\text{cal}}^\circ$ to the ICS3 or the MTCS3 are not treated by skills like normalization and average. The present theoretical *DACMe* ICSs without Born correction are listed in the sixth column. The seventh column gives the Born corrected *DACMe* ICSs in bold.

The relative percent error of the experimental partial ICS from the SMC amended experimental (full) ICS1 (with ‘c’), that from the Born SMC amended experimental (full) ICS2 (with ‘d’), and that from the Born *DACMe* amended experimental (full) ICS3 (with ‘e’) are given in the parentheses of the second column, respectively, for every scattering energy. The relative percent error of the theoretical *DACMe* ICS (without Born correction) from the SMC amended experimental ICS1 (with ‘f’), and that of the Born *DACMe* ICS from the Born *DACMe* amended experimental ICS3 (with ‘g’) are listed in the parentheses of the sixth and the seventh columns, respectively. Table 2 gives the similar errors for MTCSs.

The ICS data in table 1 indicate that: (1) the experimental partial ICSs obtained using numerical integration of experimental DCSs over scattering angles of $\theta_{\text{cal}}^\circ \rightarrow 180^\circ$ indeed carry about 20% to 100% errors due to missing the scattering information of $0^\circ \rightarrow \theta_{\text{cal}}^\circ$. (2) The absolute value of the

Table 1. Integral cross sections (in 10^{-16} cm²) of $e + \text{THF}$ at 6, 7, 8, 10, 12 15 and 20 eV based on different experimental data [12, 14].

Energy	Experimental partial ICS	Amended experimental ICSs			<i>Theoretical DACMe</i> ICS	<i>Theoretical DACMe</i> ICS with Born correction
		SMC ICS1	Born SMC ICS2	<i>Born DACMe</i> ICS3		
6 eV ^a	35.06 ($\theta_{\text{cal}}^{\circ} = 30^{\circ}$) (−40.05% ^c , −97.58% ^d , −106.65% ^e)	49.1	69.27	72.45	49.68 (−1.18% ^f)	72.41 (0.06% ^g)
7 eV ^a	39.62 ($\theta_{\text{cal}}^{\circ} = 20^{\circ}$) (−21.66% ^c)	48.2	—	—	47.22 (2.03% ^f)	—
8 eV ^a	34.21 ($\theta_{\text{cal}}^{\circ} = 25^{\circ}$) (−42.65% ^c)	48.8	—	—	49.85 (−2.15% ^f)	—
10 eV ^a	34.6 ($\theta_{\text{cal}}^{\circ} = 20^{\circ}$) (−28.9% ^c , −67.77% ^d , −44.16% ^e)	44.6	58.05	49.88	44.78 (−0.4% ^f)	50.04 (−0.32% ^g)
12 eV ^a	31.85 ($\theta_{\text{cal}}^{\circ} = 20^{\circ}$) (−39.09% ^c)	44.3	—	—	46.98 (−6.05% ^f)	—
15 eV ^a	29.03 ($\theta_{\text{cal}}^{\circ} = 20^{\circ}$) (−46.4% ^c , −70.48% ^d , −53.22% ^e)	42.5	49.49	44.48	42.81 (−0.73% ^f)	44.54 (−0.13% ^g)
20 eV ^a	27.23 ($\theta_{\text{cal}}^{\circ} = 20^{\circ}$) (−50.57% ^c , −64.74% ^d , −50.79% ^e)	41	44.86	41.06	39.56 (3.51% ^f)	40.97 (0.22% ^g)
8 eV ^b	22.72 ($\theta_{\text{cal}}^{\circ} = 25^{\circ}$) (−77.02% ^c)	40.22	—	—	41.41 (−2.96% ^f)	—
20 eV ^b	17.18 ($\theta_{\text{cal}}^{\circ} = 20^{\circ}$) (−131.08% ^d , −116.53% ^e)	—	39.7	37.2	—	37.22 (−0.05% ^g)

^a The theoretical data at this energy is calculated based on the experimental measurements of Dampc *et al* [14], and the experimental partial ICS is obtained by integrating the experimental DCSs [14] of $\theta_{\text{cal}}^{\circ}$ to 180°.

^b The theoretical data at this energy is calculated based on the experimental measurements of Colyer *et al* [12] and the experimental partial ICS is obtained by integrating the experimental DCSs [12] of $\theta_{\text{cal}}^{\circ}$ to 130°.

^c The error of the experimental partial ICS from the **SMC** amended experimental (full) ICS1.

^d The error of the experimental partial ICS from the **Born SMC** amended experimental (full) ICS2.

^e The error of the experimental partial ICS from the **Born DACMe** amended experimental (full) ICS3.

^f The error of the **DACMe** ICS without Born correction from the **SMC** amended experimental (full) ICS1.

^g The error of the **DACMe** ICS with Born correction from the **Born DACMe** amended experimental (full) ICS3.

Table 2. Momentum transfer cross sections (in 10^{-16} cm²) of $e + \text{THF}$ at 6, 7, 8, 10, 12 15 and 20 eV based on different experimental data [12, 14].

Energy	Experimental partial MTCS	Amended experimental MTCSs			<i>Theoretical DACMe</i> MTCS	<i>Theoretical DACMe</i> MTCS with Born correction
		SMC MTCS1	Born SMC MTCS2	<i>Born DACMe</i> MTCS3		
6 eV ^a	34.08 ($\theta_{\text{cal}}^{\circ} = 30^{\circ}$) (−1.53% ^c , −1.5% ^d , −4.55% ^e)	34.6	34.59	35.63	35.11 (−1.47% ^f)	35.71 (−0.22% ^g)
7 eV ^a	34.55 ($\theta_{\text{cal}}^{\circ} = 20^{\circ}$) (−1.01% ^c)	34.9	—	—	34.78 (0.34% ^f)	—
8 eV ^a	31.45 ($\theta_{\text{cal}}^{\circ} = 25^{\circ}$) (−1.75% ^c)	32.0	—	—	31.996 (0.01% ^f)	—
10 eV ^a	31.16 ($\theta_{\text{cal}}^{\circ} = 20^{\circ}$) (−0.77% ^c , −0.77% ^d , −1.16% ^e)	31.4	31.4	31.52	31.5 (−0.32% ^f)	31.56 (−0.13% ^g)
12 eV ^a	26.99 ($\theta_{\text{cal}}^{\circ} = 20^{\circ}$) (−6.34% ^c)	28.7	—	—	27.6 (3.83% ^f)	—
15 eV ^a	24.35 ($\theta_{\text{cal}}^{\circ} = 20^{\circ}$) (−3.49% ^c , −1.15% ^d , −1.52% ^e)	25.2	24.63	24.72	24.83 (1.47% ^f)	24.77 (−0.2% ^g)
20 eV ^a	21.87 ($\theta_{\text{cal}}^{\circ} = 20^{\circ}$) (−2.42% ^c , −1.23% ^d , −1.55% ^e)	22.4	22.14	22.21	22.28 (0.54% ^f)	21.98 (1.04% ^g)
8 eV ^b	18.04 ($\theta_{\text{cal}}^{\circ} = 25^{\circ}$) (−74.33% ^c)	31.45	—	—	32.9 (−4.61% ^f)	—
20 eV ^b	9.72 ($\theta_{\text{cal}}^{\circ} = 20^{\circ}$) (−95.06% ^d , −90.02% ^e)	—	18.96	18.47	—	18.46 (0.05% ^g)

^a The theoretical data at this energy is calculated based on the experimental measurements of Dampc *et al* [14], and the experimental partial MTCS is obtained by integrating the experimental DCSs [14] of $\theta_{\text{cal}}^{\circ}$ to 180°.

^b The theoretical data at this energy is calculated based on the experimental measurements of Colyer *et al* [12] and the experimental partial MTCS is obtained by integrating the experimental DCSs [12] of $\theta_{\text{cal}}^{\circ}$ to 130°.

^c The error of the experimental partial MTCS from the *SMC* amended experimental (full) MTCS1.

^d The error of the experimental partial MTCS from the *Born SMC* amended experimental (full) MTCS2.

^e The error of the experimental partial MTCS from the *Born DACMe* amended experimental (full) MTCS3.

^f The error of the *DACMe* MTCS without Born correction from the *SMC* amended experimental (full) MTCS1.

^g The error of the *DACMe* MTCS with Born correction from the *Born DACMe* amended experimental (full) MTCS3.

percent error (with ‘g’) of the Born *DACMe* ICS from the Born *DACMe* amended experimental ICS3 is less than 0.4%, and that (with ‘f’) of the *DACMe* ICS (without Born correction) from the SMC amended experimental ICS1 is less than 6.1% for every energy, which implies that the Born *DACMe* DCSs, particularly those of $0^\circ \rightarrow \theta_{\text{cal}}^\circ$, and therefore the Born *DACMe* ICSs better represent the true scattering physics of this scattering system. (3) The difference between the Born *DACMe* ICS and the *DACMe* ICS (without Born correction) is becoming smaller as scattering energy increases, and so is that between Born SMC ICS and the SMC ICS. Comparisons among small angle DCSs in figures 1 to 7 also give such an observation. This confirms the fact that the dipole scattering potential plays a very important role in low energy electron-polar molecule scattering. And such a dipole effect may be neglected for this scattering system at energies greater than 20 eV. Therefore, in the cases where the dipole included cross sections are not available at higher scattering energies, one may use the ones without dipole contributions from a credible theoretical method. The MTCS data in table 2 give similar pictures.

It is worth noting that although the ICS and the MTCS can be used as two converging standards to physically converge the theoretical DCSs, the numerical integration on DCSs over all scattering angles indeed sums over and averages all scattering angular features, and therefore hides the detailed physical differences of the DCSs obtained from using different theoretical methods.

All above *DACMe* cross sections are generated by using the experimental DCSs of Dampc *et al* [14] which are extended out to 180 degrees. In order to test the feasibility and the practicability of the *DACMe* method to the experimental DCSs which do not have the data in scattering angles $\theta^\circ < \theta_{\text{cal}}^\circ$ and $\theta^\circ > 130^\circ$, this study also performed *DACMe* calculations using the measured DCSs of Colyer *et al* [12] for this scattering system at 8 and 20 eV as examples. The *DACMe* DCSs and the experimental data [12] are listed in tables A9, A10 of the SD for 8 and 20 eV, respectively. In the last two lines of both tables 1 and 2, the experimental partial ICSs and MTCSs are generated by integrating the measured DCSs of Colyer *et al* in angles of $\theta_{\text{cal}}^\circ \rightarrow 130^\circ$. The theory amended experimental ICS and the MTCS are obtained by integrating the known theoretical (SMC, or Born SMC or Born *DACMe*) DCSs of $0^\circ \rightarrow \theta_{\text{cal}}^\circ$ and $130^\circ \rightarrow 180^\circ$, and the measured DCSs [12] of $\theta_{\text{cal}}^\circ \rightarrow 130^\circ$.

In figures 8 and 9, the hollow circles (○) are Colyer *et al*'s experimental DCSs in scattering angles $\theta_{\text{cal}}^\circ < \theta^\circ < 130^\circ$. The double-dots-dashed curve (— · — · —) in figure 8 at 8 eV presents the *DACMe* DCSs which are obtained using SMC amended experimental ICS1 and MTCS1 as converging requirements, and the one in figure 9 at 20 eV presents the Born corrected *DACMe* DCSs obtained using Born SMC amended experimental ICS2 and MTCS2 as converging requirements. All other curves are as the corresponding ones of figure 1. It can be seen from both figures that the measured data (○) of Colyer *et al* [12] are generally smaller than the experimental DCSs (●) of Dampc and coworkers [14].

Table A9 and figure 8 show that the *DACMe* DCSs at 8 eV excellently reproduce each corresponding experimental data (black solid curve matches (●)) and double-dots-dashed curve (— · — · —) matches (○), respectively. Although there are no measured data (○) of Colyer *et al* [12] available for angles $\theta^\circ > 130^\circ$, the *DACMe* (double-dots-dashed curve) still predict meaningful DCSs which have values within the error bar of other measured data (●) of Dampc and coworkers [14].

The Born corrected *DACMe* DCSs in table A10 and figure 9 at 20 eV present the same agreement quality with both measured data as those in figure 8. The excellent agreement between the Born corrected *DACMe* ICS and the Born *DACMe* amended experimental (full) ICS3 (of the last line of table 1) at this energy also indicates that the predicted *DACMe* DCSs of both $\theta^\circ < \theta_{\text{cal}}^\circ$ and $\theta^\circ > 130^\circ$ correctly give the values and physical shape of the unknown DCSs in these angular regions.

4. Summary

This study improves the DCM method [26] by introducing an algebraic technique to enhance the computational efficiency of the DCM protocol, and applies the *DACMe*—the improved DCM—to predict the DCSs of electron scattering from a THF molecule at 6, 7, 8, 10, 12, 15 and 20 eV based on a set of accurate experimental data. The study shows that the *DACMe* DCSs (with Born correction for dipole potentials) not only excellently reproduce all accurate experimental data [12, 14], but also correctly predict the numerical values and the detailed physical shapes of all DCSs that may not be given experimentally or may carry non-negligible errors from other theoretical methods. Studies on cross sections also verify the understanding that the dipole polarization potential makes significant contributions to the electron-polar molecule scattering in small angle and at low energy regions. This study indicates that the DCM/*DACMe* not only works excellently for small molecules [26] but also for important biomolecules, and that the DCM/*DACMe* is independent of the stereochemistry structure and the size of a scattering molecule. Studies also indicate that the computational speed of the *DACMe* is more than 110 times faster than that of the original DCM on a normal PC and therefore the *DACMe* greatly enhances the computational efficiency.

Extensive quantum scattering studies on electron scattering from many inorganic/organic molecules using various scattering methods have shown their power in obtaining good theoretical cross sections and in explaining physical pictures of scattering systems. However, there are still many situations where complicated scattering wave-functions and delicate scattering potentials of a given scattering system generate satisfactory cross sections at some scattering angles or energies, but may give less satisfactory or even incorrect data at some other angles or energies.

The *DACMe* method can work as an alternative to provide correct DCSs that may not be available experimentally or may not be accurately given by some theoretical methods, although it indeed does not provide a scattering potential

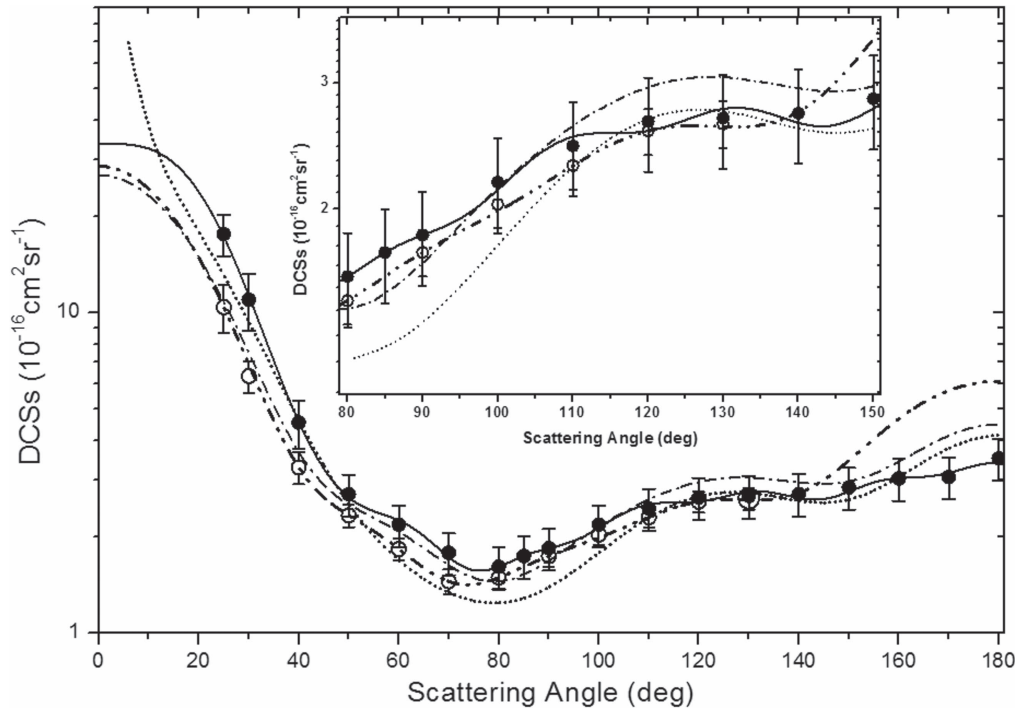


Figure 8. Elastic *DACMe* DCSs of $e + \text{THF}$ at 8 eV based on different experimental DCSs. Full circles (●), experiment data of Dampc *et al* [14]; black solid curve (—), presents *DACMe* based on the experimental data of Dampc *et al*; hollow circles (○), experimental data of Colyer *et al* [12]; double-dots-dashed curve (— · —), presents *DACMe* based on the experimental data of Colyer *et al* [12]. Both *DACMe* DCSs (solid curves, without Born correction) are obtained using the SMC amended experimental ICS1 and MTCS1 as converging requirements; dot-dashed curve (— · —), SMC calculation [18]; dotted curve (···), from the complex Kohn variational method [21].

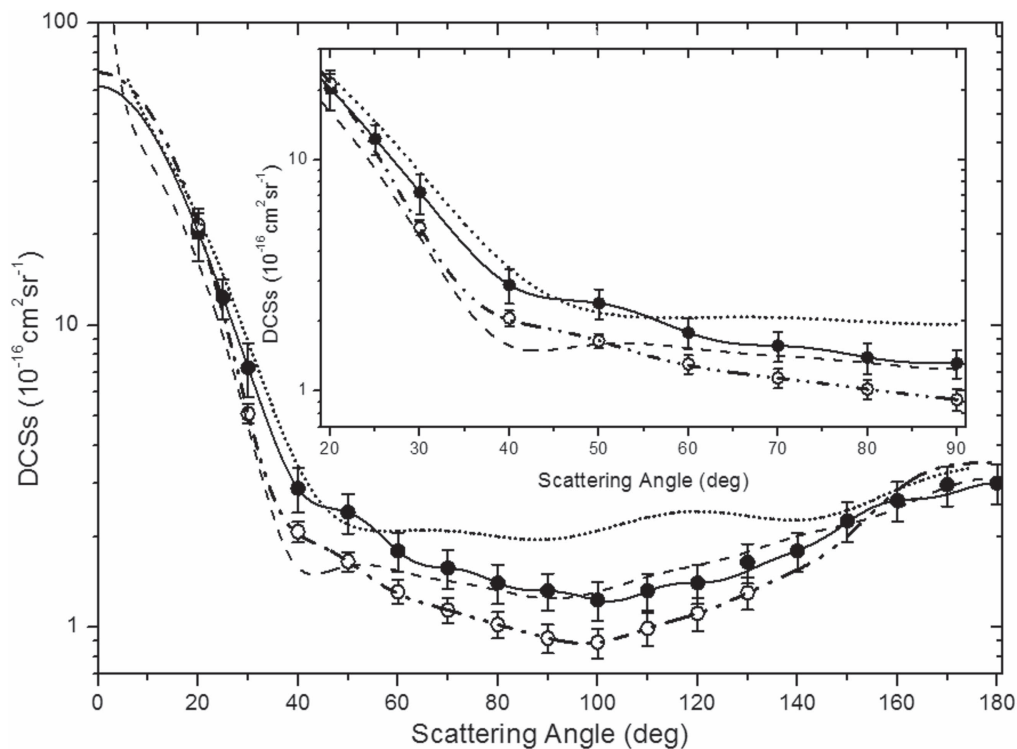


Figure 9. Elastic *DACMe* DCSs of $e + \text{THF}$ at 20 eV based on different experimental DCSs. Full circles (●), experiment data of Dampc *et al* [14]; black solid curve (—), presents Born corrected *DACMe* based on the experimental data of Dampc *et al*; hollow circles (○), experimental data of Colyer *et al* [12]; double-dots-dashed curve (— · —), presents Born corrected *DACMe* based on the experimental DCSs of Colyer *et al*. Both Born corrected *DACMe* DCSs (solid curves) obtained using the Born SMC amended experimental ICS2 and MTCS2 as converging requirements; dashed curve (— · —), Born corrected SMC calculations [19]; dotted curve (···), from the complex Kohn variational method [21].

picture. The *DACMe* may work as an easy and economic theoretical supplement in cases where correct scattering cross section data are demanded.

Acknowledgments

This work was supported by the Research Fund of Key Disciplines of Atomic and Molecular Physics, Xihua University, and the Fund of the Research Center of Laser Fusion, CAEP, P R C. We are grateful to Mariusa Zubek and Irenusz Linert for providing their tabulated experimental DCS results, and we also thank Professor Carl Winstead and Professor Stephen Buckman for their experimental and theoretical data.

References

- [1] Boudaiffa B, Cloutier P, Hunting D, Huels M A and Sanche L 2000 *Science* **287** 1658
- [2] Huels M A, Boudaiffa B, Cloutier P, Hunting D and Sanche L 2003 *J. Am. Chem. Soc.* **125** 4467
- [3] Sonntag C 1997 *The Chemical Basis of Radiation Biology* (London: Taylor and Francis)
- [4] Lepage M, Letarte S, Michaud M, Motte-Tollet F, Hubin-Franskin M J, Roy D and Sanche L 1998 *J. Chem. Phys.* **109** 5980
- [5] Maljkovic J 2014 *J. Phys.: Conf. Ser.* **565** 012005
- [6] Sanche L 2005 *Eur. Phys. J. D* **35** 367
- [7] Denifl S, Ptasinska S, Cingel M, Matejcik S, Scheier P and Mark T D 2003 *Chem. Phys. Lett.* **377** 74
- [8] Aflatooni K, Scheer A M and Burrow P D 2006 *J. Chem. Phys.* **125** 054301
- [9] Linert I, King G C and Zubek M 2004 *J. Electron Spectrosc. Relat. Phenom.* **134** 1
- [10] Thiemer B, Andreesen J R and Schraeder T 2003 *Arch. Microbiol.* **179** 266
- [11] Milosavljevic A R, Giuliani A, Sevic D, Hubin-Franskin M J and Marinkovic B P 2005 *Eur. Phys. J. D* **35** 411
- [12] Cloyer C J, Vizcaino V, Sullivan J P, Brunger M J and Buckman S J 2007 *New J. Phys.* **9** 41
- [13] Lemelin V, Bass A D, Cloutier P and Sanche L 2016 *J. Chem. Phys.* **144** 074701
- [14] Dampc M, Milosavljevic A R, Linert I, Marinkovic B P and Zubek M 2007 *Phys. Rev. A* **75** 042710
- [15] Bremner L J, Curtis M G and Walker C I 1991 *J. Chem. Soc. Faraday Trans.* **87** 1049
- [16] Allan M 2007 *J. Phys. B: At. Mol. Opt. Phys.* **40** 3531
- [17] Homem M G P, Sugohara R T, Sanches I P, Lee T M and Iga I 2009 *Phys. Rev. A* **80** 032705
- [18] Winstead C and McKoy V 2006 *J. Chem. Phys.* **125** 074302
- [19] Gauf A, Hargreaves L R, Jo A, Tranner J, Walls T, Winstead C and McKoy V 2012 *Phys. Rev. A* **85** 052717
- [20] Mozejko P and Sanche L 2005 *Radiat. Phys. Chem.* **73** 77
- [21] Trevisan C S, Orel E A and Rescigno T N 2006 *J. Phys. B: At. Mol. Opt. Phys.* **39** L255
- [22] Fuss M C, Sanz A G, Blanco F, Limao-Vieira P, Brunger M J and Garcia G 2014 *Eur. Phys. J. D* **68** 161
- [23] Garland A N, Brunger J M, Garcia G, de Urquijo J and White R D 2013 *Phys. Rev. A* **88** 062712
- [24] Bouchiha D, Gorfinkel J D, Caron L G and Sanche L 2006 *J. Phys. B: At. Mol. Opt. Phys.* **39** 975
- [25] Fuss M, Mu A, Oller J C, Blanco F, Almeida D, Limao-Vieira P, Do T P D, Brunger M J and Garcia G 2009 *Phys. Rev. A* **80** 052709
- [26] Sun W G, Wang Q, Zhang Y, Li H, Feng H and Fan Q C 2015 *J. Phys. B: At. Mol. Opt. Phys.* **48** 125201
- [27] Gianturco F A, Di Martino V and Jain A 1992 *Nuovo Cimento D* **14** 411
- [28] Gianturco F A, Sanna N and Sarno R 1995 *Computational Methods for Electron-Molecule Collisions* ed W Huo and F Gianturco (New York: Plenum) ch 5
- [29] Arfken G 1985 Legendre functions *Mathematical Methods for Physicists* 3rd edn (Orlando, FL: Academic Press) ch 12
- [30] Morrison M A and Sun W G 1995 *Computational Methods for Electron-Molecule Collisions* ed W Huo and F Gianturco (New York: Plenum) ch 6